Bull. Mater. Sci. (2021) 44:123
https://doi.org/10.1007/s12034-021-02409-2

Synthesis and visible-light photocatalytic activity of brookite/BiOBr

ZHITENG WANG[1], NING LIU[1], HUIDONG XIE[1,*], JIE LI[1], YAJUAN ZHAO[1] and NA WANG[2]

[1] School of Chemistry and Chemical Engineering, Xi'an University of Architecture and Technology, Xi'an 710055, China
[2] College of Architecture and Civil Engineering, Xi'an University of Science and Technology, Xi'an 710054, China
*Author for correspondence (xiehuidong@tsinghua.org.cn)

MS received 13 December 2019; accepted 1 January 2021

Abstract. Brookite TiO_2 was synthesized and BiOBr was supported on the surface of brookite TiO_2 by a hydrothermal method. X-ray diffraction and X-ray photoelectron spectroscopy analyses of the composites confirmed the formation of brookite TiO_2/BiOBr. Transmission electron microscopy results confirmed the as-prepared composites were nano-sized. The optimum loading amount of BiOBr was 30%. The photocatalytic results show that the degradation efficiency of rhodamine B by titanite TiO_2/BiOBr (30%) under visible-light irradiation for 2 h is close to 100%. $^{\bullet}O_2^-$ and h^+ are the main active species during the photocatalytic process. The improvement of photocatalytic activity might be because the formation of p–n hetero-junction enhanced the separation efficiency of photogenerated electron–hole pairs. The photocurrent density of the brookite/BiOBr (30%) was about 2 times higher than that of pure brookite.

Keywords. Brookite TiO_2; BiOBr; photocatalysis; rhodamine B; degradation.

1. Introduction

With the development of industry, the deterioration of the environment has become a main problem that we must face. The photocatalysis of semiconductors is considered to be an ideal 'green strategy' to deal with the increasingly serious environmental pollution in modern society. TiO_2 is a widely used n-type semiconductor [1,2], because it has no toxicity, high photocatalytic activity and high photochemical stability [3,4]. There are three crystal structures of TiO_2, which are anatase, brookite and rutile [5]. Ohtani *et al* [6] have shown that the photocatalytic activity of brookite TiO_2 is higher than anatase and rutile. However, due to the inherent large bandgap, TiO_2 can only absorb ultraviolet (UV) light and has high photogenerated electron–hole combination and low photocatalytic efficiency, which limits its practical application. In order to solve these problems, researchers have enhanced the photocatalytic performance of TiO_2 by forming a hetero-junction of TiO_2 with other semiconductors. Particularly, designing p–n hetero-junctions is of significance because of the existence of an internal electric field, which can greatly accelerate the separation of photogeneration electron–hole and ultimately improve the photocatalytic activity [7,8]. Therefore, it is of great importance to seek a p-type semiconductor with a reasonable bandgap, which can combine n-type TiO_2 in the process of photocatalytic degradation [9–12].

BiOX (X = F, Cl, Br, I) compounds are new functional materials developed in recent years [13–16]. Their layered structure, excellent adsorption performance and photocatalytic properties have attracted wide attentions of many researchers. In addition, BiOBr has a series of advantages of eco-friendliness, nontoxicity and low cost in the treatment of pollutant in wastewater [17–20]. Wang *et al* [9] developed BiOBr nanosheets-decorated amorphous TiO_2 nanofibres hierarchical structure and found the optimal p-BiOBr/n-TiO_2 nanofibres exhibited excellent photocatalytic degradation and of rhodamine B (RhB) and MO under UV-light irradiation with a high recyclability. Jia *et al* [21] deposited the BiOBr nanosheets well on the outer wall of anatase TiO_{2-x} nanotubes by chemical bath deposition method. The as-prepared TiO_2/BiOBr at 80°C exhibits good visible-light photocatalytic activities with a degradation percentage of 70% for 100 min and a stable performance for RhB. Up to now, there are no reports on the properties of brookite/BiOBr.

In this study, single-phase of brookite and the brookite/BiOBr composite photocatalyst were prepared by hydrothermal method. The optimal preparation conditions of brookite/BiOBr composites were investigated. The morphology and photoelectron spectroscopy of the composite were measured. All the photocatalytic degradation of RhB was performed under a 70-W metal halide lamp irradiation with a 420 nm cutoff filter.

Published online: 30 April 2021

2. Experimental

2.1 *Materials, reagents and instruments*

All the chemicals were of analytical grade, including: titanium tetrachloride (Tianjin Damao Chemical Reagent Factory), sodium hydroxide (Tianjin Beilian Fine Chemicals Development Co., Ltd.), cetyl trimethyl bromide ammonium (Tianjin Zhiyuan Chemical Reagent Co., Ltd.), bismuth nitrate pentahydrate (Sinopharm Chemical Reagent Co., Ltd), P25 (Degussa), and potassium bromide (Sinopharm Chemical Reagent Co., Ltd).

The phases of the products were characterized using a Rigaku 9000 X-ray diffractometer (XRD, Japanese Physiology) with a Cu Kα radiation operating at 40 kV, 40 mA and scanning speed 10° min^{-1}. The microstructure and morphology of the samples were analysed by a JEM-2100F transmission electron microscopy (TEM, JEOL Company, Japan) operated at 200 kV. The diffuse reflectance spectra (DRS) were measured by a PE Lambd1050 UV-vis spectrometer (Perkin Elmer Company, USA). The photoluminescence (PL) spectra were measured by a F-320 fluorescent spectrophotometer (Tianjin Gangdong Co. Ltd., China). The photoelectron spectra were conducted by an ESCALAB 250xi X-ray photoelectron spectroscopy (XPS, ThermoFisher Scientific Company, USA).

2.2 *Preparation of photocatalysts*

2.2a *Preparation of brookite titania:* The preparation method of brookite was hydrothermal, the process was similar to the method described in reference [22]. Briefly, titanium tetrachloride ($TiCl_4$) was used as a raw material and cetyltrimethyl ammonium bromide (CTAB) was used as a soft template. They were mixed together and then NaOH solution was slowly dropped into the mixtures to adjust the pH to 10. The hydrothermal reaction was conducted at 220°C for 22 h. After the reaction completed, the white precipitate was washed thoroughly with deionized water and ethanol, and then dried at 80°C for 4 h.

2.2b *Preparation of brookite/BiOBr:* The brookite/BiOBr composite photocatalyst was prepared by a hydrothermal method. The main preparation process was as follows: a certain amount of bismuth nitrate pentahydrate was dissolved in deionized water to obtain suspension A; stoichiometric potassium bromide was dissolved in deionized water with stirring to form solution B; solution B was slowly dripped into suspension A, and the above-prepared brookite was slowly added to the mixture. Finally, the suspension was transferred to a 100 ml autoclave and reacted at 160°C for 8 h. After the reaction, the products were washed with deionized water, anhydrous ethanol and dried at 80°C for 5 h. The effects of the mass percentage of BiOBr to brookite, which was 5, 10, 20, 30 and 40% on the degradation efficiency, were studied.

2.3 *Photocatalytic activity measurement*

Rhodamine B was used to evaluate the photocatalytic performance. In a typical process, 0.1 g photocatalyst and 200 ml of 10 mg l^{-1} RhB solution were added to a 250 ml quartz beaker. To ensure the establishment of adsorption–desorption equilibrium between the photocatalyst and RhB, the suspension was stirred in the dark for 20 min before the light turned on. A 70 W metal halide lamp (Philips Lighting Electrical Appliance) with a 420 nm cutoff filter was used to supply the visible-light irradiation. Samples were taken at interval of 20 min and centrifuged at 8000 rpm for 10 min. The change in the concentration of RhB was monitored by measuring the absorbance at λ_{max} (554 nm) with a UV-6100PC (SXL-1100M) vis spectrophotometer. The following formula was used to calculate the degradation percentage of RhB by photocatalysts:

$$\text{Degradation percentage, } D\,(\%) = \frac{A_e - A_t}{A_e}\% \qquad (1)$$

where the measured absorbance of the pristine RhB solution was A_0, the absorbance of solution after balance of the adsorption and desorption was A_e, and the absorbance of solution after irradiation for a certain time was A_t.

2.4 *Electrochemical performance test*

Transient photocurrent (*i–t*) curves of catalysts were measured at a CHI660E electrochemical workstation (Shanghai Chenhua Instruments Co., Ltd.). Using three-electrode system, the sample to be measured was coated on FTO glass to make as working electrode, Pt plate was used as counter electrode, and calomel electrode was used as reference electrode. The electrolyte solution was 0.3 M Na_2SO_4. A 35 W LED lamp (Shuaiyang Lighting Company) was used as the light source. The preparation of the working electrode was as follows: 5 mg photocatalyst and 25 µl 5% Nafion solution were mixed in 0.475 ml ethanol to obtain a uniform slurry by ultrasonic dispersion. The slurry was coated on FTO glass and dried at 80°C for more than 12 h.

3. Results and discussion

3.1 *Characterization of the photocatalysts*

3.1a *XRD:* The phase of the as-prepared samples was investigated by powder XRD. Figure 1 shows the XRD patterns of the as-prepared brookite and brookite/BiOBr (30%) composites. The prepared brookite is well crystallized and its diffraction peaks are in good

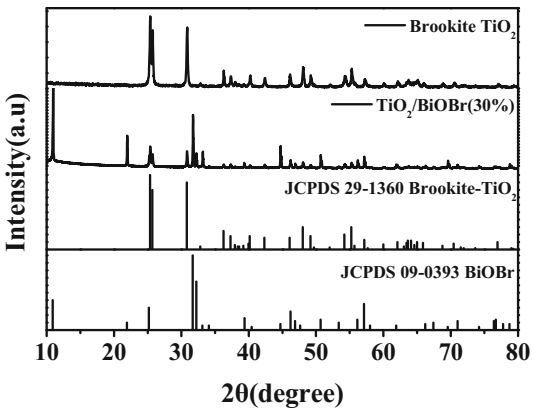

Figure 1. XRD patterns of brookite and brookite/BiOBr (30%) composites.

agreement with the phase of brookite TiO_2 (JCPDS 29-1360). For brookite/BiOBr (30%) composite, the diffraction peaks at about 13.3°, 24.3°, 34.3°, 35.7° and 47.3° can be indexed to the (001), (002), (012), (110) and (020) planes of tetragonal phase BiOBr (JCPDS 09-0393) [23], respectively, indicating that the brookite/BiOBr composite has been successfully prepared. As brookite is not stable, it is necessary to determine whether the crystalline form of brookite has been changed in the subsequent composite process and whether small amount of anatase is formed. Anatase has a special diffraction peak at 2θ of 62.57° [24] and 75.0° [25], which do not overlap with the peaks of brookite, so we can identify whether there is anatase in the brookite by the two peaks. As shown in the figure, no diffraction peaks at these two angles are observed, indicating there are no anatase in the composite.

3.1b *TEM:* The morphology of the as-prepared brookite/BiOBr (30%) composites was further observed by TEM. Figure 2a shows a spindle shape, which is confirmed to be brookite by elemental analysis. The dark-field TEM image in figure 3b shows a spiral plate structure, about 1 μm long, like the wings of a butterfly, which is proved to be BiOBr by elemental analysis. The distance between the stripes in the high-resolution TEM (HRTEM) image in figure 2c is about 0.371 nm, which corresponds to the {201} plane of brookite. Figure 2d gives the selected-area electron diffraction (SAED) of the brookite/BiOBr (30%). The calculated distances of r_1 and r_3 are 6.90 and 4.1 1 nm^{-1}, which correspond to interplanar spacing 0.24 nm for the $\{\bar{1}02\}$ and 0.14 nm for the {600} planes of brookite, respectively. By measuring the angles between r_1 and r_2 or r_2 and r_3 (shown in the figure), the indexes of r_1, r_2 and r_3 were determined and shown in the figure. The angles are in good agreement with the theoretical values.

3.1c *XPS:* To display chemical composition and chemical states of the brookite/BiOBr (30%) nanocomposite, a survey XPS spectra were employed and shown in figure 3. In this binding energy range, the peaks of Ti2p, O1s, Br3d and Bi4f are detected, which demonstrate the formation of the nanocomposite. The C1s signals usually originate from the carbon contamination during XPS measurements [26].

Figure 4 displays the high-resolution XPS spectra of Ti2p, O1s, Br3d and Bi4f of the brookite/BiOBr (30%) nanocomposite. In figure 4a, the peaks of Ti2p peaked at 458, 464 and 467 eV are caused by $Ti2p_{3/2}$ and $Ti2p_{1/2}$ [27] of Ti^{4+}. The binding energy is same as that of brookite, indicating that Ti is combined with oxygen instead of carbon [28,29]. The O1s spectrum in figure 4b can be deconvoluted into three peaks 529.6, 530.3 and 530.9 eV [30,31]. The peak at 529.6 eV can be ascribed to two types of oxygen: the lattice oxygen in the $[Bi_2O_2]^{2+}$ layers of BiOBr or the O_v defects in the TiO_2 matrix [30,32]. The O_v will lead to accelerating faster charge transfer and lower recombination of electron–hole pairs [33]. The peak at 530.3 eV corresponds to O1s in Ti–O bond of brookite [34], whereas the peak at 530.9 eV corresponds to Ti–OH bonding [35]. In figure 4c, two strong peaks at 158.8 and 164.1 eV can be assigned to the $Bi4f_{7/2}$ and $Bi4f_{5/2}$ because of forming the Bi–O bond in BiOBr lattice [36]. The peaks of Br3d at 68.5 and 69.5 eV in figure 4d are in agreement with $Br3d_{5/2}$ and $Br3d_{3/2}$, respectively [37]. Obviously, the XPS elemental analysis are well consistent with the results of XRD and TEM, further confirming the formation of brookite/BiOBr (30%).

3.2 *Photocatalytic performance of the as-synthesized photocatalyst*

Figure 5a is time-dependent degradation curve of RhB by brookite/BiOBr with different mass ratios of BiOBr. Under the experimental conditions, the effect of dark adsorption and photocatalysis without catalyst can be neglected. With the increase of BiOBr content, the degradation ratio increased first and then decreased. When the BiOBr content is 30%, the degradation ratio of the composites is the highest, reaching 100% for 120 min. The decrease of the photocatalytic activity is probably due to the high proportion of BiOBr, which will change the structure, composition and morphology of the catalysts. Figure 5b is a comparison of photocatalytic degradation of RhB by brookite/BiOBr (30%), brookite, BiOBr and commercial P25. It can be found that the photocatalytic degradation efficiency of brookite/BiOBr (30%) is greater than the other three photocatalysts.

Figure 6 is degradation percentages of RhB by brookite/BiOBr (30%) under different pH. The pH of RhB solution was adjusted by 0.1 mol l^{-1} HCl solution or 0.1 mol l^{-1} NaOH. As can be seen from figure 6, the degradation percentage is highest under acidic condition pH = 3. The pH of the solution has a great influence on the photocatalytic process. On one hand, the pH can

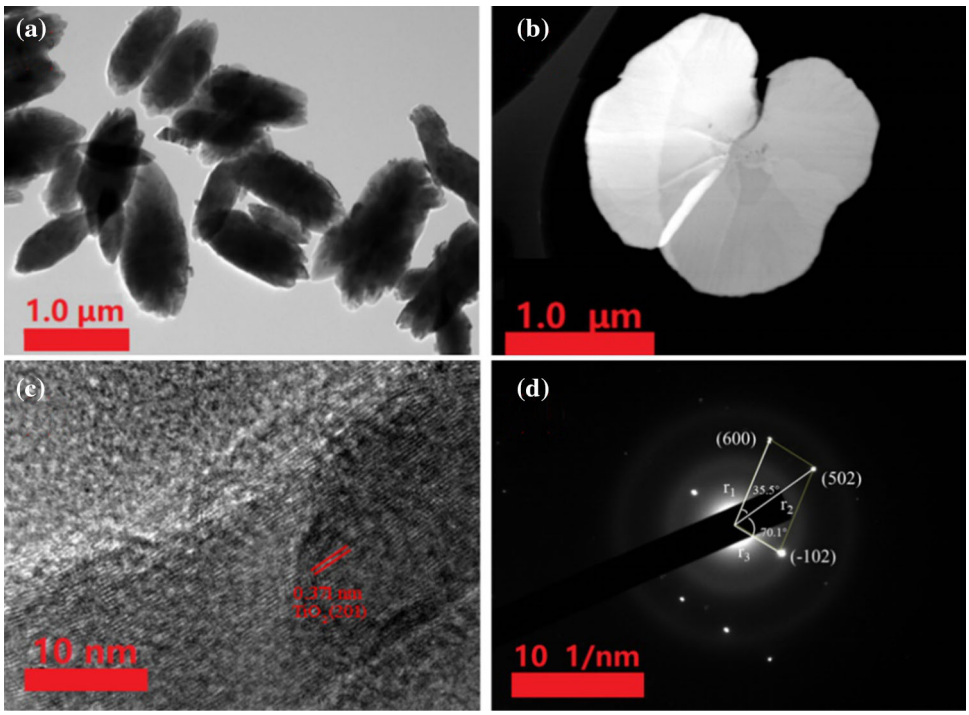

Figure 2. TEM analysis of the brookite/BiOBr (30%) nanocomposite. (**a**) Bright-field TEM image shows brookite; (**b**) dark-field TEM image shows BiOBr; (**c**) HRTEM image shows brookite; (**d**) SAED pattern of brookite.

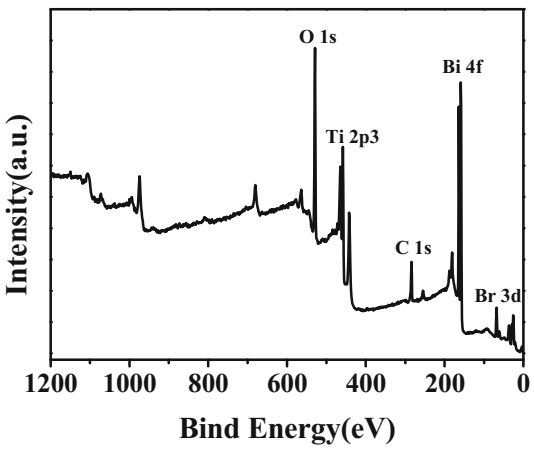

Figure 3. XPS survey spectra of the brookite/BiOBr (30%) composite.

affect the charge on the organic dyes, and thus affect the catalytic degradation efficiency. RhB is a kind of cationic dye, which is easy to be adsorbed by the photocatalyst in acid condition and easy to be degradated. On the other hand, the pH can affect the generation of active species. According to the Nernst equation, a low pH is profitable for the generation of $^{\bullet}O_2^-$ and $^{\bullet}OH$, and thus profitable for the photodegradation.

3.3 *Detection of active species*

In order to further study the photocatalytic degradation mechanism of RhB, active species trapping experiments were carried out. Benzoquinone (BQ), isopropanol (IPA) and EDTA-2Na were used as scavengers for the detection of superoxide radicals ($^{\bullet}O_2^-$), hydroxyl radicals ($^{\bullet}OH$) and holes (h^+), respectively. Figure 7 shows the time-dependent degradation percentage of RhB by brookite/BiOBr (30%) with adding different capturing agents. Clearly seen from the figure, the degradation ratios of RhB are greatly inhibited by BQ. Also, when EDTA-2Na is added, the degradation efficiency decreased significantly. Unlike BQ and EDTA-2Na, the addition of IPA has less influence on the degradation efficiency of RhB. The results show that $^{\bullet}O_2^-$ and h^+ are the main active species involved in the visible-light photocatalytic degradation of RhB.

3.4 *UV–vis diffuse reflectance spectra of SBN*

Figure 8a shows the diffuse reflectance spectra of brookite TiO_2, BiOBr and brookite/BiOBr (30%). Brookite TiO_2 has absorption in the ultraviolet region ($\lambda < 385$ nm), while BiOBr has absorption in the visible-light region ($\lambda <$ 437 nm). The bandgap energy, E_g, of the brookite TiO_2

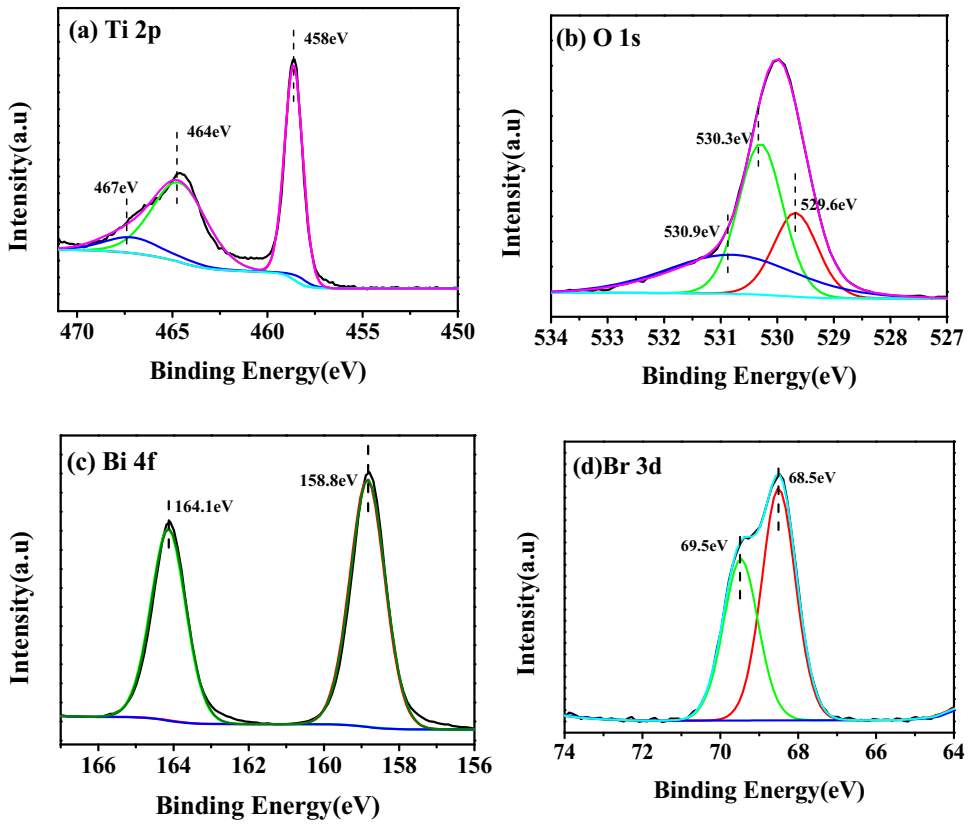

Figure 4. XPS high-resolution spectra of the brookite/BiOBr (30%) composite. (**a**) Ti2p; (**b**) O1s; (**c**) Bi4f and (**d**) Br3d.

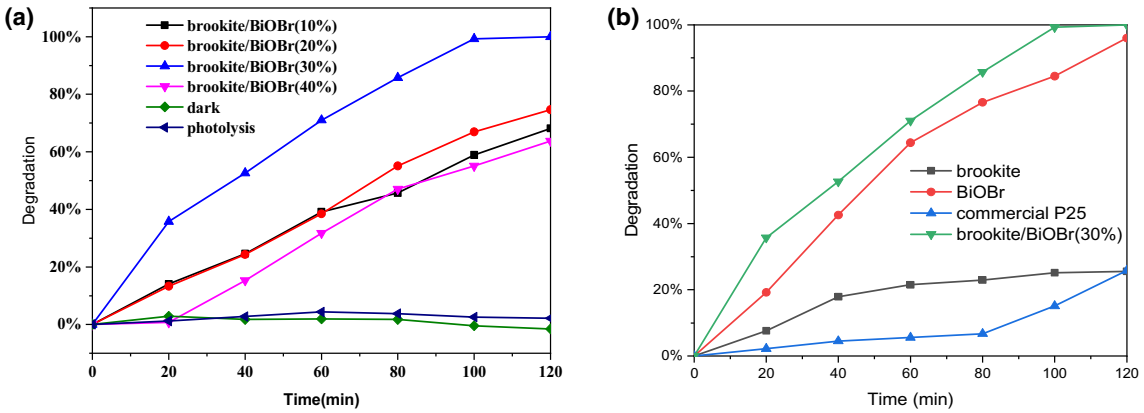

Figure 5. Degradation ratios of RhB *vs.* time under different conditions. (**a**) Brookite with different BiOBr content; (**b**) comparison of brookite/BiOBr (30%), brookite, BiOBr and commercial P25.

and BiOBr can be calculated according to the following formula (2):

$$\alpha h\nu = (Ah\nu - E_g)^{n/2} \quad (2)$$

where α, h, ν, A, E_g are the absorption coefficient, Planck constant, light frequency, proportional constant and band-gap energy (eV) of the semiconductor, respectively. For indirect-type semiconductors of brookite TiO_2 and BiOBr, n is equal to 4. Figure 8b shows the $(\alpha h\nu)^{1/2}$–hν curves of brookite TiO_2 and BiOBr. The bandgap E_g can be obtained by the intersection of the extending linear part of the curves and the x-axis. As shown in the figure, the bandgap E_g of brookite TiO_2 and BiOBr are 3.10 and 2.72 eV, respectively, which were very close to values in the Refs [38,39].

3.5 *PL spectra*

The photogenerated electron (e^-) and hole (h^+) of the semiconductors can be generated under the light excitation.

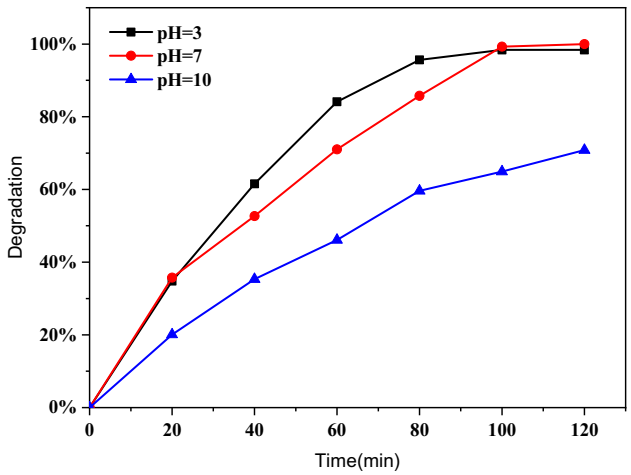

Figure 6. Degradation percentages of RhB by brookite/BiOBr(30%) under different pH.

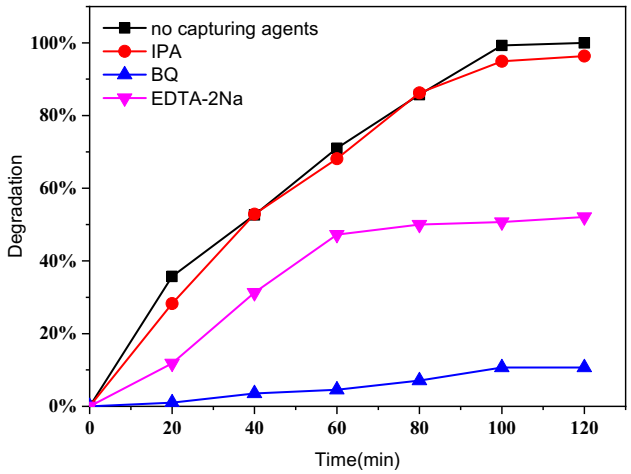

Figure 7. Effects of capturing agents on photocatalytic degradation activity of brookite/BiOBr (30%).

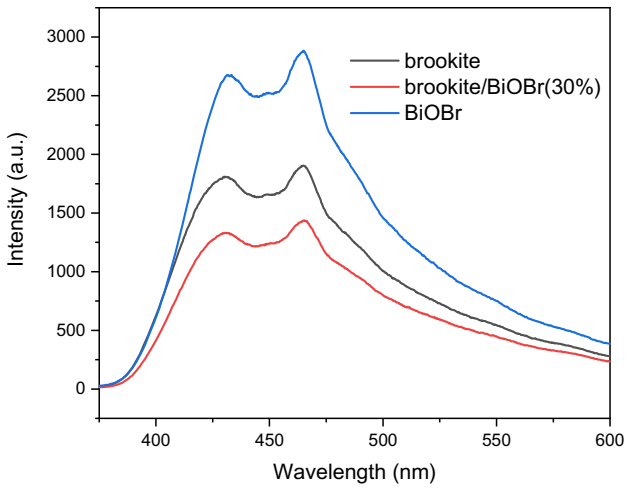

Figure 9. Photoluminescence spectra of brookite TiO_2, BiOBr and brookite/BiOBr (30%).

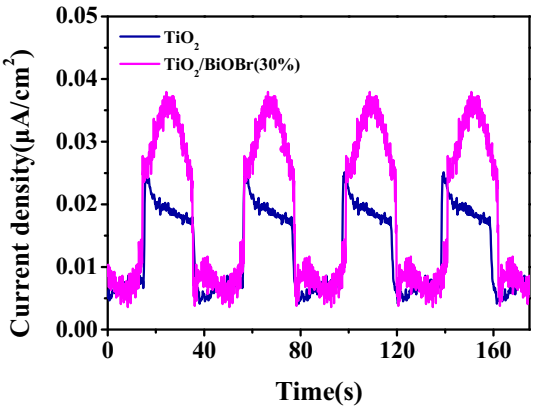

Figure 10. Transient photocurrent curves of brookite and brookite/BiOBr (30%).

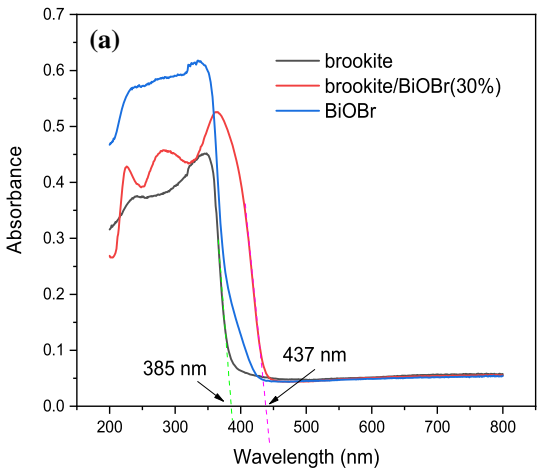

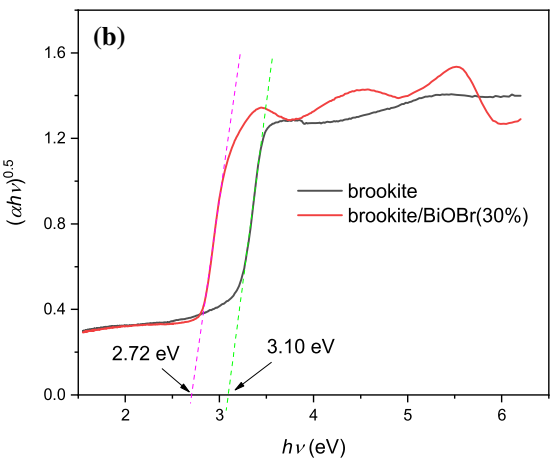

Figure 8. (**a**) Diffuse reflectance spectra of brookite TiO_2, BiOBr and brookite/BiOBr (30%), (**b**) $(\alpha h\nu)^{1/2}$–$h\nu$ curves of brookite TiO_2 and BiOBr.

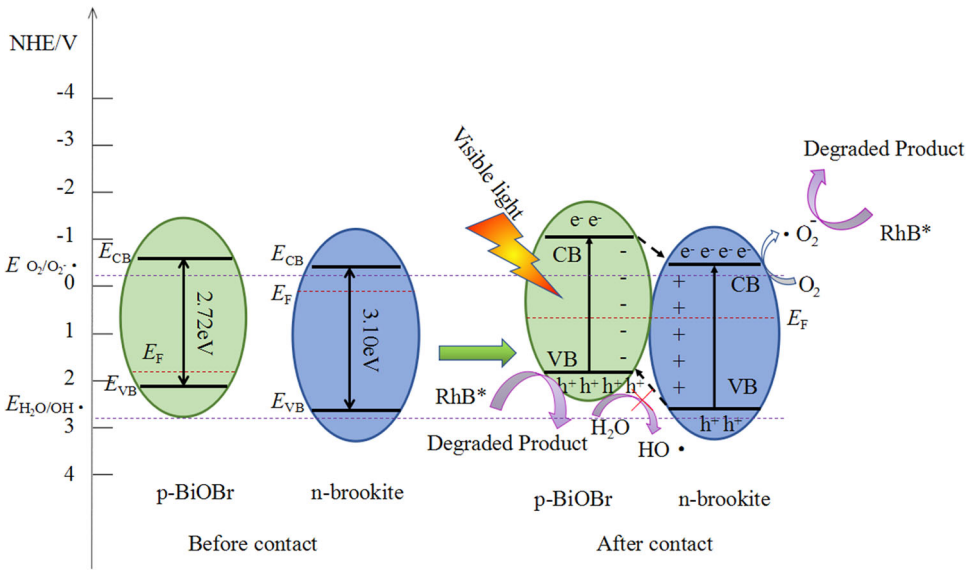

Figure 11. Schematic illustration of the photocatalytic mechanism and the formation of the p–n hetero-junction between brookite and BiOBr.

The recombination of electron and hole will result in the fluorescence emission. Figure 9 shows the PL spectra of brookite TiO_2, BiOBr and brookite/BiOBr (30%) excited at 320 nm. It can be seen that the shapes of the PL spectra of all the catalysts are very similar. There are two strong peaks in the range of 350–600 nm. The intensity of brookite/BiOBr (30%) composite is weaker than that of pure brookite TiO_2 and BiOBr, which indicates that the recombination of the photogenerated electron and hole of the brookite/BiOBr (30%) is lower. This is consistent with the experimental results of photodegradation of RhB.

3.6 *Photocurrent responses*

Transient photocurrent curves reflect the characteristics of photogenerated carriers produced by semiconductor electrodes under the excitation of light. In the test, a 35-W white LED is used as the light source and the distance between the light source and the working electrode is 13 cm. The working electrode was shaded at intervals of 20 s. Figure 9 shows the *I–t* curves of the as-prepared photocatalysts of brookite and brookite/BiOBr (30%) measured with no voltage. The instantaneous response and photocurrent stability of the photocatalysts to visible light can be observed. The photocurrent density of brookite/BiOBr (30%) increases obviously and its photocurrent density is about 2 times higher than that of brookite, which is in accordance with its excellent photocatactivity.

3.7 *Photocatalytic degradation mechanism*

According to the active species measured in the photodegradation process and the relative band levels of brookite and BiOBr, the photocatalytic mechanism was proposed and shown in figure 11. As reported, brookite is an n-type semiconductor whose Fermi level is near its conduction band (CB), whereas BiOBr is a p-type semiconductor whose Fermi level is near its valence band (VB). The reported E_{CB} and E_{VB} of the brookite are 0.50 and 2.6 eV, respectively. For BiOBr, its E_{CB} and E_{VB} are –0.63 and 2.09 eV, respectively [21]. When they contact each other, a p–n hetero-junction will be formed. The hole diffuses from p-BiOBr to n-brookite, while the electron diffuses from n-brookite to p-BiOBr. Thus, a built-in electrical potential in the space charge region from brookite to BiOBr will form after equilibrium. The bands of BiOBr will move upward and the bands of brookite move downward to allow the Fermi levels equilibrate [40]. Because E_{VB} of BiOBr is less positive than that of $H_2O/OH^{\bullet}$(+2.72 eV *vs.* NHE), the production of $OH^{\bullet}$ becomes impossible. Thus, the holes will directly oxidize RhB on the surface of BiOBr. At the same time, E_{CB} of brookite is more negative than that of $O_2/^{\bullet}O_2^-$ (–0.33 eV *vs.* NHE), so $^{\bullet}O_2^-$ can form on the surface of brookite to oxidize RhB. The construction of p–n junctions in the composite decreases the recombination rate of photoinducted electro–hole pairs, while will enhance the photocatalytic performance. This is also consistent with the results of free radical detection experiments.

4. Conclusion

In summary, brookite and BiOBr were prepared by hydrothermal method and they were composited by hydrothermal method. The prepared catalyst was confirmed to be a nano-scale photocatalyst by TEM analysis. The brookite/BiOBr composite improved the photocatalytic

performance of degrading RhB. The catalyst has excellent catalytic activity for degrading RhB solution. Under visible-light irradiation of 70-W metal halide lamp, the degradation ratio of RhB by brookite/BiOBr (30%) can exceed 90% for 100 min. $^{\bullet}O_2^-$ and h^+ are the main active species in the photodegradation process of RhB. The formation of p–n hetero-junction in the brookite/BiOBr (30%) enhanced its photocatalytic performance. The high degradation ratio indicates that this composite has a great potential as an effective photocatalyst.

Acknowledgements

This research was supported by the National Natural Science Foundation of China under grant no. 51708447 and Natural Science Foundation of Shaanxi Province under grant no. 2018JM2022.

References

[1] Huang C, Lv Y, Zhou Q, Kang S, Li X and Mu J 2014 *Ceram. Int.* **40** 7093
[2] Li Y L, Liu Y M, Wang J S, Uchaker E, Zhang Q F, Sun S B *et al* 2013 *J. Mater. Chem. A* **1** 7949
[3] Lee E J, An A K, He T, Woo Y C and Shon H K 2016 *J. Membrane Sci.* **520** 145
[4] Mahy J, Lambert S, Leonard G, Zubiaur A, Olu P-Y, Mahmoud A *et al* 2016 *J. Photoch. Photobio. A* **329** 189
[5] Bokhimi X, Morales A, Aguilar M, Toledo-Antonio J A and Pedraza F 2001 *Int. J. Hydrogen Energ.* **26** 1279
[6] Ohtani B, Handa J I, Nishimoto S I and Kagiya T 1985 *Chem. Phys. Lett.* **120** 292
[7] Wang K X, Shao C L, Li X H, Zhang X, Lu N, Miao F J *et al* 2015 *Catal. Comm.* **67** 6
[8] Song X C, Li W T, Huang W Z, Zhou H, Zheng Y F and Yin H Y 2015 *Mater. Chem. Phys.* **160** 251
[9] Wang K X, Zhang Y S, Liu L N, Lu N and Zhang Z Y 2019 *J. Mater. Sci.* **54** 8426
[10] Kumar M, Singh R and Som T 2018 *Appl. Surf. Sci.* **428** 1006
[11] Qian L L, Li Y, Li J F and Wang C W 2018 *Superlattice Microst.* **117** 317
[12] Scuderi V, Amiard G, Sanz R, Boninelli S, Impellizzeri G and Privitera V 2017 *Appl. Surf. Sci.* **416** 885
[13] Henle J, Simon P, Frenzel A, Scholz S and Kaskel S 2007 *Chem. Mater.* **19** 366
[14] Ganose A M, Cuff M, Butler K T, Walsh A and Scanlon D O 2016 *Chem. Mater.* **28** 1980
[15] Gao B, Zhang J R, Chen L, Guo J K, Shen S, Au C T *et al* 2019 *Appl. Surf. Sci.* **492** 157
[16] Zhang W J, Fu J, Wang Y, Zhang X X and Li J L 2019 *Optik* **176** 448
[17] Xu J, Li L, Guo C S, Zhang Y and Wang S F 2013 *Chem. Eng. J.* **221** 230
[18] Wang X J, Yang W Y, Li F T, Zhao J, Liu R H, Liu S J *et al* 2015 *J. Hazard. Mater.* **292** 126
[19] Shang M, Wang W Z and Zhang L 2009 *J. Hazard. Mater.* **167** 803
[20] Zhang D, Li J, Wang Q G and Wu Q S 2013 *J. Mater. Chem. A* **1** 8622
[21] Jia L X, Tan X, Yu T and Zhang Z 2018 *Mater. Res. Bull.* **105** 322
[22] Zou Y L, Tan X, Yu T, Li Y, Shang Q Q and Wang W L 2014 *Mater. Lett.* **132** 182
[23] Qun Y L, Jin Y L, Zhuo J, Tian Y P and Ling Z 2013 *Appl. Catal. B Environ.* **142–143** 1
[24] Hu W B, Li L P, Li G S, Tang C L and Lang S 2009 *Cryst. Growth Des.* **9** 3676
[25] Zhao B, Lin L and He D 2013 *J. Mater. Chem. A* **1** 1659
[26] Rashid J, Abbas A, Chang L C, Iqbal A, Haq I U, Rehman A *et al* 2019 *Sci. Total Environ.* **665** 668
[27] Wang D H, Jia L, Wu X L, Lu L Q and Xu A W 2012 *Nanoscale* **4** 576
[28] Feng T, Zhang G Z, Wang Y Q, Gao C T, Chen L L, Peng Z *et al* 2014 *Appl. Surf. Sci.* **320** 703
[29] Chandra M R, Rao T S, Pammi S V N and Sreedhar B 2015 *Mater. Sci. Semicon. Proc.* **30** 672
[30] Fu R R, Zeng X Q, Ma L, Gao S M, Wang Q Y, Wang Z Y *et al* 2016 *J. Power Sources* **312** 12
[31] Zou J, Gao J C and Wang Y W 2009 *J. Photoch. Photobio. A Chem.* **202** 128
[32] Zhu S R, Wu M K, Zhao W N, Yi F Y, Tao K and Han L 2017 *J. Solid State Chem.* **255** 17
[33] Li G, Lian Z, Li X, Xu Y, Wang W, Zhang D *et al* 2015 *J. Mater. Chem. A* **3** 3748
[34] Duan Y W, Chen X W, Zhang X X, Xiang W and Wu C F 2018 *Solid State Sci.* **86** 12
[35] Ming W G, Yu W H, Yi C L, Chao T Y, Yu Y X, Fitzmorris R C *et al* 2011 *Nano Lett.* **11** 3026
[36] Li H P, Liu J Y, Liang X F, Hou W G and Tao X T 2014 *J. Mater. Chem. A* **2** 8926
[37] Li W B, Zhang Y P, Bu Y Y and Chen Z Y 2016 *J. Alloys Compd.* **680** 677
[38] Lin H F, Li L P, Zhao M L, Huang X S, Chen X M, Li G S *et al* 2012 *J. Am. Chem. Soc.* **134** 8328
[39] Mehraj O, Mir N A, Pirzada B M and Sabir S 2015 *Appl. Surf. Sci.* **332** 419
[40] Ao H, Wang K D, Wang P F, Wang C and Hou J 2016 *Appl. Catal. B Environ.* **194** 157